ACS APPLIED MATERIALS & INTERFACES

Open Access

This article is licensed under CC-BY-NC-ND 4.0

www.acsami.org Research Article

Transmission Electron Microscopy Analysis of the Microstructure of Nanocrystalline Small-Molecule Semiconductors in Functional Organic Thin-Film Transistors

Simon Hettler,* Ute Zschieschang, Hagen Klauk, Martin Peterlechner, and Yolita M. Eggeler

Cite This: *ACS Appl. Mater. Interfaces* 2026, 18, 18073−18081

Read Online

ACCESS | Metrics & More | Article Recommendations | Supporting Information

ABSTRACT: Transmission electron microscopy has been employed to investigate the microstructure of nanocrystalline vacuum-deposited thin films of the small-molecule organic semiconductor 2,9-diphenyl-dinaphtho[2,3-b:2′,3′-f]thieno[3,2-*b*]-thiophene (DPh-DNTT) in functional bottom-gate organic thin-film transistors (TFTs) using both cross-sectional and plan-view specimens. Since the charge transport in organic TFTs is confined to the first molecular layer adjacent to the interface with the gate dielectric, the microstructure of this first molecular layer is of critical importance for the TFT performance, and transmission electron microscopy (TEM) is the most powerful technique to analyze this buried molecular layer. Direct imaging reveals that the DPh-DNTT molecules are oriented edge-on with their long axis in the vertical configuration with respect to the gate dielectric surface. An additional phase in which the DPh-DNTT molecules are oriented in the face-on configuration is observed in the protrusions that typically form in vacuum-deposited DPh-DNTT thin films; however, this face-on configuration is found only on top of layers in which the DPh-DNTT molecules are in the edge-on configuration. This suggests that the edge-on configuration serves as a template for the growth of the face-on configuration.

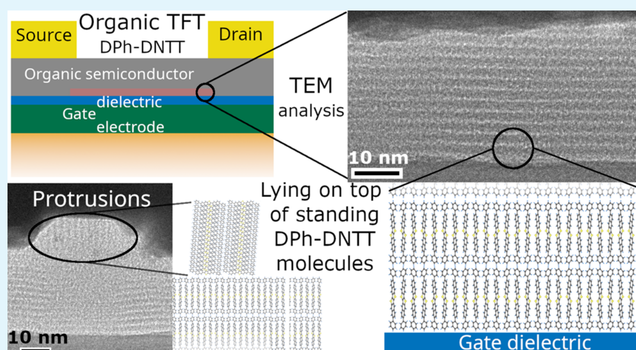

KEYWORDS: *organic thin-film transistors, transmission electron microscopy, molecular crystal, microstructure, templated growth*

INTRODUCTION

The performance of organic electronic devices is intrinsically linked to the properties of the organic semiconductor employed as the active material.[1,2] In organic thin-film transistors (TFTs), similar to their inorganic counterparts, the application of a gate-source voltage leads to the formation of a conductive channel in the semiconductor layer between the source and drain contacts. In organic TFTs, the mobility of the charge carriers in the organic semiconductor thin film is therefore an essential characteristic. This mobility is dependent on the shape and properties of the individual molecules of the organic semiconductor and, more importantly, on the organization and orientation of these molecules in the thin film, i.e., on the microstructure of the organic semiconductor layer. Due to the confinement of the charge transport to the first few nm adjacent to the interface with the gate dielectric,[3] the knowledge of the microstructure within this buried molecular layer is crucial for understanding the performance of organic TFTs.

Several analysis techniques have been used to characterize organic semiconductor thin films to link their structure to the measured electrical performance of the corresponding organic TFT. Scanning electron microscopy (SEM) and atomic force microscopy (AFM) are typically applied to characterize the surface topography.[4] Scanning tunneling microscopy (STM) in combination with low energy electron diffraction (LEED) has been used to elucidate the growth mechanism on metal surfaces.[5] X-ray diffraction (XRD) allows studying the crystal structure of the organic semiconductors on a macroscopic scale,[4] and grazing incident wide-angle X-ray scattering (GIWAXS) is an efficient technique to study both the structure and orientation of large single crystals such as monolayer molecular crystals (MMCs).[6] Transmission electron microscopy (TEM) is a technique frequently used to obtain site-specific structural information on organic thin films with high spatial resolution by both imaging and diffraction techniques.[7] Most investigations focused on the analysis of plan-view specimens, where the organic thin film is grown directly on carbon-based TEM grids[8−11] or is floated onto a TEM grid.[12] These investigations are limited by electron beam

Received: January 27, 2026
Revised: March 4, 2026
Accepted: March 5, 2026
Published: March 18, 2026

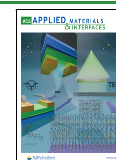

Downloaded via KIT BIBLIOTHEK on April 23, 2026 at 11:16:19 (UTC).
See https://pubs.acs.org/sharingguidelines for options on how to legitimately share published articles.

ACS Publications
© 2026 The Authors. Published by American Chemical Society

https://doi.org/10.1021/acsami.6c01886
ACS Appl. Mater. Interfaces 2026, 18, 18073−18081

damage of the organic material and the critical dose was shown to be linked to the melting temperature of the molecules.[7] Additionally, the preparation of cross-sectional lamellae by conventional preparation techniques based on Ar^+ ion milling,[13,14] ultramicrotomy,[15] or focused ion beam (FIB)[16,17] provides a means for characterization of the first molecular layer of the organic semiconductor film located directly on the gate dielectric surface, in which the charges are transported from source to drain in bottom-gate organic TFTs. However, such analyses can be found only scarcely in literature,[18] revealing for example the structure of a pentacene thin film.[16] The reason for the infrequent analysis of cross-sectional specimens by TEM might be the damage induced by the ion beam and, maybe more critically, by the electron beam leading to an amorphization of the organic semiconductor material during TEM specimen preparation by FIB.[19] Indeed, several publications show cross-sectional TEM images of organic TFTs, where the organic semiconductor was damaged and appears with an amorphous structure.[1,12,20]

2,9-Diphenyl-dinaphtho[2,3-b:2′,3′-f]thieno[3,2-*b*]-thiophene (DPh-DNTT) has been shown to be one of the most stable and best-performing organic semiconductors for p-channel organic TFTs with intrinsic channel mobilities larger than 7 $cm^2V^{-1}s^{-1}$.[21−24] Figure 1 shows a sketch of the DPh-DNTT molecule and the corresponding molecular crystal structure in views along different crystallographic directions.[21] Similar to most molecules employed in organic TFTs based on vacuum-deposited small-molecule organic semiconductors, the DPh-DNTT molecules have a sticklike or rod-like shape (Figure 1a), which leads to a unit cell of the corresponding crystal with one long and two shorter axes. The long axis of the molecule corresponds to the [001] crystal direction, with a length of c = 2.43 nm (Figure 1b). The crystal structure is monoclinic with α = 94.3°, as seen from Figure 1b. The [100] and [010] lattice parameters a = 0.761 nm and b = 0.618 nm are similar, but not equal (Figure 1d), implying that the molecular crystal has a low symmetry. Generally, the DPh-DNTT and related molecules are believed to grow with the [001] axis in vertical orientation on insulating substrates such as the gate dielectric of bottom-gate TFTs, i.e., the molecules grow edge-on, i.e., are "standing" on the substrate (see sketch in Figure 1e). Very recently, AFM analyses with high spatial resolution have shown that some DPh-DNTT molecules also appear in the face-on or horizontal (Figure 1e) configuration with the [001] axis parallel to the substrate surface.[25] These analyses indicated that this configuration is found in the protrusions ("nanosprouts"), which frequently form in DPh-DNTT thin films. However, AFM is a purely surface-sensitive technique, and the question whether the molecules grow in the face-on configuration only on top of a layer with the edge-on configuration or also directly on the surface of the gate dielectric has so far not been answered convincingly. A microscopic explanation of the excellent electrical performance of DPh-DNTT TFTs is therefore still missing and requires further analysis of this structure−property relationship. Due to the nanocrystalline structure of vacuum-deposited DPh-DNTT films, macroscopic techniques such as XRD or GIWAXS are not able to answer this question.

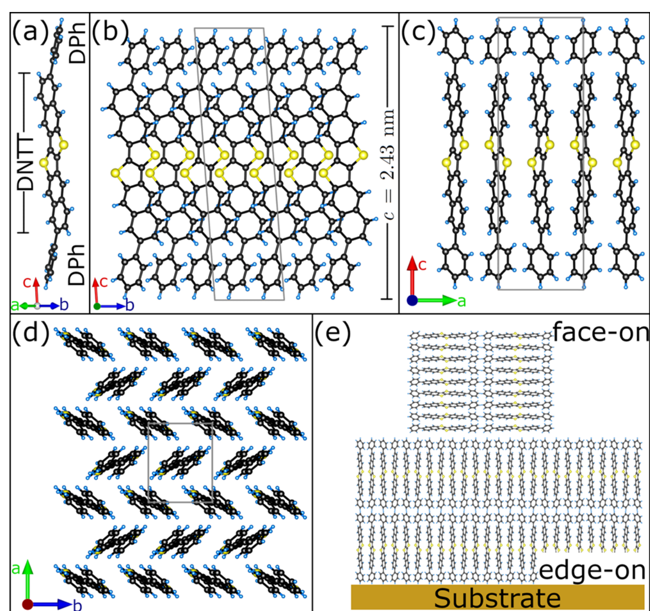

Figure 1. Sketches of the crystal structure of the DPh-DNTT molecular crystal along different crystallographic directions.[21] Green, blue, and red arrows indicate the a/[100], b/[010], and c/[001] axes, respectively. (a) View of a single DPh-DNTT molecule in [110] projection revealing the central conjugated DNTT core and the two terminal phenyl substituents, which show a rotation around the c axis with respect to the DNTT core. (b−d) View of the crystal along the [100], [010], and [001] crystallographic directions, respectively. The views in (a−c) reveal the large lattice parameter c in [001] direction as indicated in (b), corresponding to the length of the molecule, in comparison to the smaller size of the unit cell in the a,b plane as seen in (d). (e) Sketch of the face- and edge-on configurations of the DPh-DNTT molecules in nanocrystalline vacuum-deposited thin films with respect to the substrate.

In this work, TEM, scanning (S)TEM and energy-dispersive X-ray (EDX) analyses were conducted on vacuum-deposited DPh-DNTT thin films with two different thicknesses and in two complementary geometries using both cross-sectional lamellae prepared directly from functional organic TFTs and plan-view specimens made of DPh-DNTT films grown on TEM grids. The experimental results show that the DPh-DNTT molecules adopt an edge-on configuration on the surface of the gate dielectric of the TFTs. The resulting crystalline films are composed of nanoscale grains with characteristic sizes of only a few tens of nanometers. Moreover, the emergence of domains with the face-on molecular configuration is identified, which are found only within protruding features on top of the initial vertically oriented molecular layer. This is attributed to a templated growth mechanism similar to what has been observed and is exploited with MMCs.[26]

RESULTS AND DISCUSSION

Cross-Sectional Analyses of the Functional DPh-DNTT Layer

Structural Analysis by High-Resolution TEM. Figure 2 shows experimental results obtained from a TEM cross-sectional analysis of a functional DPh-DNTT TFT with a measured effective charge-carrier mobility of μ_{eff} = 4 $cm^2V^{-1}s^{-1}$ (see Figure S1 in the Supporting Information (SI)). A TEM image at an intermediate resolution is shown in Figure 2a and reveals the layer system of the organic TFT made up (from bottom to top) of the Si substrate, the Al gate electrode, the AlO_x/self-assembled monolayer (SAM) gate dielectric, the DPh-DNTT organic semiconductor, Au source/drain contacts,

https://doi.org/10.1021/acsami.6c01886
ACS Appl. Mater. Interfaces 2026, 18, 18073−18081

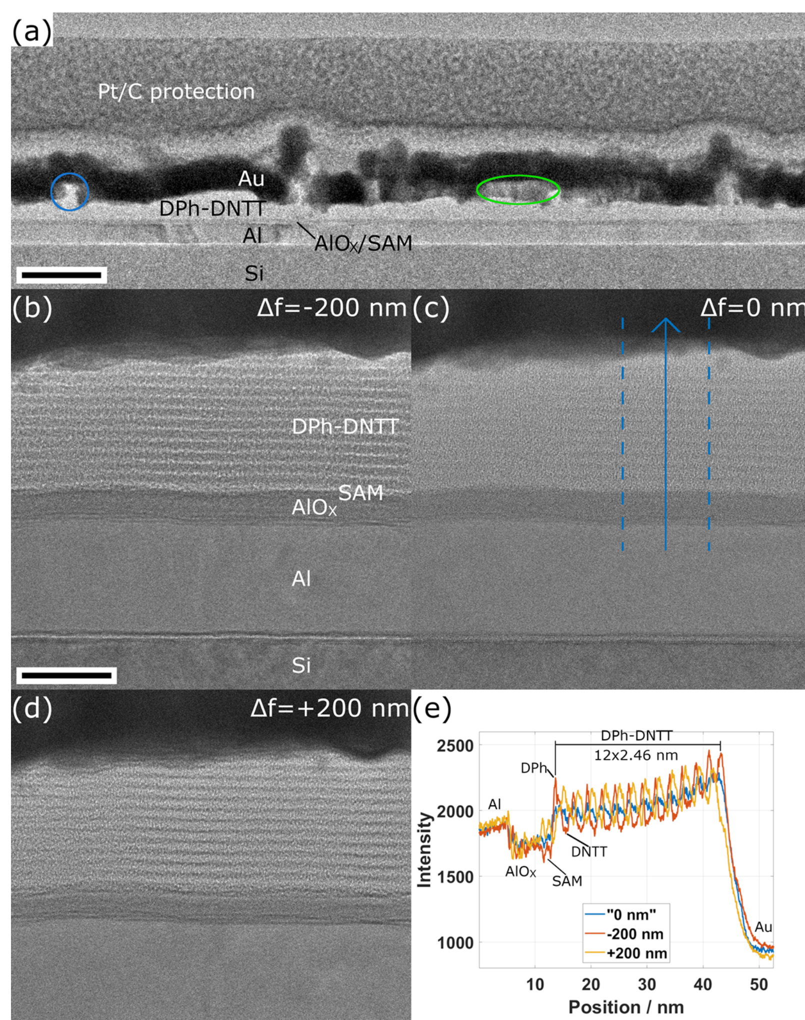

Figure 2. TEM analysis of a DPh-DNTT TFT. (a) TEM image at an intermediate resolution (the scale bar is 100 nm), revealing the layer system of the device, as labeled in the image. The blue circle highlights a pillar of DPh-DNTT grown on top of a continuous layer. The green ellipse indicates a region with intermediate dark contrast generated by an overlap of Au and DPh-DNTT layers across the lamella thickness. (b,d) HRTEM images of the identical sample region for different defocus values as indicated, again revealing the layer system and additionally horizontal lines in the DPh-DNTT thin film. The blue dashed lines and arrows indicate the position for the line profile generation. The scale bar is 20 nm. (e) Comparison of three line profiles taken from the images shown in (b) red line, (c) blue line, and (d) yellow line. Twelve fringes with a periodicity of 2.46 nm can be measured in the DPh-DNTT layer. Two fringes are seen at the interface to the AlO_x layer, which are attributed to the *n*-tetradecylphosphonic acid SAM.

and the Pt/C protection layer deposited during specimen preparation. At this magnification, the single-crystalline Si substrate appears with homogeneous contrast, while several nanosized crystal grains can be distinguished in the Al gate electrode due to diffraction contrast. The gate dielectric appears as a fine layer with slightly darker contrast on top of the Al gate electrode.

The organic semiconductor layer is continuous but exhibits a considerable thickness variation on the scale of 10−100 nm, including small protrusions on top of the continuous layer. One such protrusion has been indicated by a blue circle in Figure 2a. This morphology agrees with SEM analyses of DPh-DNTT thin films from literature[25,27] and with results presented later on in this manuscript. As the underlying AlO_x layer appears completely flat, the inhomogeneous thickness of the DPh-DNTT layer must originate from the growth of the DPh-DNTT layer. The morphology of the DPh-DNTT layer then translates into a similar roughness of the Au layer on top of the DPh-DNTT film. In several areas, the interface between the bright DPh-DNTT and the dark Au layer is not sharp, and regions with an intermediate gray-level intensity are seen (green ellipse in Figure 2a). This is explained by a thickness variation of the DPh-DNTT layer within the TEM lamella in the direction of the electron beam, causing overlap of both layers and the observed intermediate contrast.

More information about the DPh-DNTT layer structure can be gained from high-resolution (HR)TEM images. Three HRTEM images of the identical specimen region but acquired under different imaging conditions are depicted in Figure 2b−d. Again, the layer system of the Si substrate, Al gate electrode, AlO_x/SAM gate dielectric, DPh-DNTT organic semiconductor, and Au source/drain contact is revealed. At this magnification, individual atomic columns can be distinguished in the Si substrate oriented in [110] direction. Also, the surface of the AlO_x/SAM gate dielectric exhibits some minor roughness, with variations below 1 nm in magnitude. The contrast in these underlying layers as well as in the Au covering layer is only marginally affected by the application of different

https://doi.org/10.1021/acsami.6c01886
ACS Appl. Mater. Interfaces 2026, 18, 18073−18081

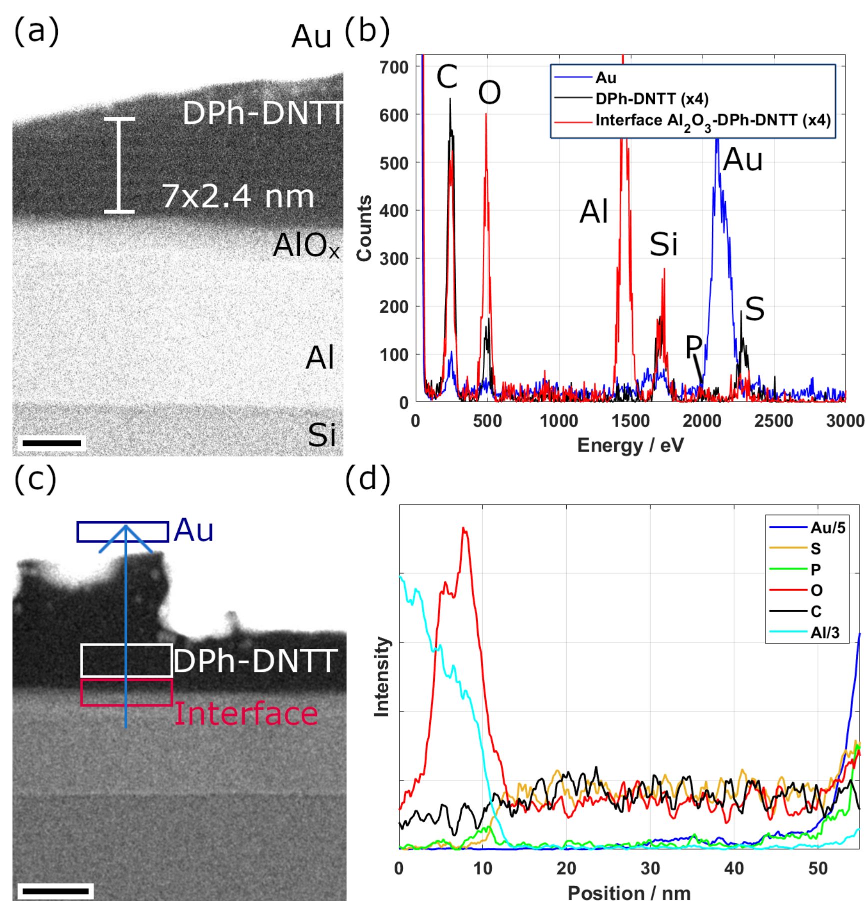

Figure 3. STEM and EDX analyses of cross-sectional lamella of a DPh-DNTT TFT. (a) HAADF-STEM image showing the layer system of the Si substrate, Al gate electrode, AlO_x/SAM gate dielectric, DPh-DNTT organic semiconductor, and Au source/drain contact. Horizontal lines with a periodicity of 2.4 nm are seen, confirming the edge-on configuration of the DPh-DNTT molecules. The scale bar is 10 nm. (b) Comparison of three EDX spectra acquired from three different areas from the Au source/drain contact (blue curve), the DPh-DNTT film (black curve), and its interface with the gate dielectric (red curve). The areas are marked in (c). The spectra from the DPh-DNTT film and the interface regions have been multiplied by 4 to allow a better comparison. (c) HAADF-STEM survey image for STEM-EDX analyses. The regions of the spectra shown in (b) and the position of the line profile shown in (d) are indicated. The scale bar is 20 nm. (d) Line profile across the layers showing the intensity of the EDX lines of Au (blue, divided by 5), S (yellow), P (green), O (red), C (black), and Al (light blue, divided by 3). See the text for discussion.

defocus values Δf of (b) −200 nm, (c) approximately 0 nm, and (d) + 200 nm. In contrast, a strong contrast change is observed in the DPh-DNTT film. Under focused conditions (Figure 2c), the layer exhibits alternating horizontal lines with weak dark and bright contrast. These lines become more clearly visible when defocus is applied (Figure 2b,d). The contrast of the lines is inverted when the sign of the defocus is changed, which is best visible from the comparison of line profiles shown in Figure 2e. These line profiles have been taken from the three aligned images across the layer system, as indicated by the blue arrow in Figure 2c. The periodicity of the fringes seen in the DPh-DNTT layer is determined to be 2.46 nm, which corresponds well with the [001] lattice parameter c of the DPh-DNTT crystal (2.43 nm, see Figure 1b).

The observed defocus-induced contrast changes are caused by the image-formation mechanism in HRTEM. The contrast in HRTEM images of thin specimens consisting of lighter elements is governed by the phase contrast, and this phase contrast is strongly influenced by the applied defocus value. Figure S2 in the Supporting Information shows a plot of phase-contrast transfer functions (PCTFs) for the three defocus values employed here and the parameters of the microscope. The PCTF indicates, in dependence of the spatial frequency, how information present in the electron wave after transmitting the specimen is transferred to phase contrast in the image. The values of $\Delta f = \pm$ 200 nm are large for HRTEM standards and lead to strong oscillations for higher spatial frequencies (small distances in the image). The contrast of the atomic columns in the Si substrate is therefore not directly interpretable. However, up to the spatial frequency at which the PCTF reaches its first zero (1.6 nm^{-1}, 0.625 nm real space distance for $\Delta f = \pm200$ nm), the information is transferred with the same sign and an interpretation is possible. Thereby, a negative/positive defocus value (under-/overfocus) leads to a dark/bright contrast of an object with a positive potential such as an atom.[28] As the spatial frequency corresponding to the [001] lattice parameter of the DPh-DNTT crystal (0.41 nm^{-1}, 2.43 nm) is well below this first zero, the observed contrast in Figure 2b−d indeed makes it possible to gain more information on the specimen. To understand the contrast, the projected potential of the DPh-DNTT crystal was calculated (see Figure S3, Supporting Information). The calculations show that the positive potential is higher in the conjugated core (the DNTT section) of the molecule when compared to the phenyl (DPh) substituent sections attached to either end of the molecule. The conjugated core will

https://doi.org/10.1021/acsami.6c01886
ACS Appl. Mater. Interfaces 2026, 18, 18073−18081

therefore appear with a dark contrast in underfocus and a bright contrast in overfocus conditions. As the line profile shows an initial maximum in the DPh-DNTT layer for underfocus conditions (red line in Figure 2e), this maximum can be identified as the phenyl substituents of the molecules and thus confirms that the first molecular layer is found edge-on on the AlO_x gate dielectric, and no DPh-DNTT molecules are found to be face-on on the surface of the gate dielectric.

The analysis of the 12 fringes shows that in the analyzed area, 12 unit cells of the DPh-DNTT molecular crystal are oriented edge-on on top of the gate dielectric, which corresponds to a film thickness of 29 nm, smaller than the nominal layer thickness of 40 nm. In addition to these fringes, two additional maxima are seen at the interface to the AlO_x layer for overfocus conditions (Figure 2d and the yellow line in Figure 2e), which correspond to minima for underfocus (Figure 2b and the yellow line in Figure 2e). These features cannot be attributed to amorphous AlO_x, which does not show a variation in the contrast for the different defocus values. The overall step in the contrast between the AlO_x layer and the DPh-DNTT layer suggests that the extrema do not correspond to the DPh-DNTT molecules either. Instead, it can be linked to the *n*-tetradecylphosphonic acid SAM, which is part of the hybrid AlO_x/SAM gate dielectric and is allowed to form on the AlO_x surface prior to growth of the DPh-DNTT film. The *n*-tetradecylphosphonic acid molecule has a length of 1.95 nm[29] and forms SAMs with a thickness of 1.7 nm, as measured by X-ray reflectivity.[30] The width of the two extrema in the line profile (Figure 2e) is measured to be 1.8 nm, which is in reasonable agreement with the length of the *n*-tetradecylphosphonic acid molecule and the measured thickness of the SAMs.

The detailed HRTEM image analysis thus makes it possible to identify all layers involved in the TFT fabrication process, including the *n*-tetradecylphosphonic acid SAM. Additionally, it is confirmed that the initial DPh-DNTT layer grows in the edge-on configuration ([001] direction parallel to the surface normal), which is the desired orientation for lateral field-effect transistors.[31,32] Two additional HRTEM images confirm that this orientation is consistently found throughout the first molecular layer (Figure S4, Supporting Information). Figure S5, Supporting Information, shows three images of an additional cross-sectional specimen prepared from a substrate with the same layer system but with a smaller thickness of the DPh-DNTT film of nominally 8 nm as opposed to 40 nm. For this smaller thickness, the DPh-DNTT film is not continuous. However, the DPh-DNTT molecules are still consistently found in the edge-on configuration, confirming that the initial growth on the gate dielectric occurs in this orientation.

It is of interest to analyze the size of the domains in which the fringes in the DPh-DNTT film appear with a similar contrast. For example, the fringe contrast is found to decrease in the left part of the HRTEM images in Figure 2b−d, which indicates a change in orientation with respect to the right part, which was used to generate the line profiles. These differences can be linked to the presence of a grain boundary between two nanosized grains. As the horizontal fringes continue across this grain boundary, the [001] crystal direction does not change between these grains, and the molecules are continuously in the edge-on configuration. The molecular crystal merely exhibits a rotation around the [001] direction between these grains. The small size of the domains in the range of 50 nm suggests that the DPh-DNTT thin film has a nanocrystalline microstructure, which will be analyzed in more detail below.

Compositional Analysis by STEM and EDX. Figure 3 shows STEM imaging and spectroscopy results obtained from a second lamella prepared from a DPh-DNTT TFT. The STEM beam current was set to 1 pA for these measurements to minimize beam damage and allow an analysis of the device in its pristine state. An HAADF-STEM image is displayed in Figure 3a, which again reveals the layer system of the device. As the contrast in HAADF-STEM images is approximately proportional to $Z^{1.7}$,[33] the Au layer appears with high intensity. The contrast settings of the image were adjusted to saturate the Au layer so that contrast variations in the underlying layers become visible. Below the Au layer, a dark layer is seen, which corresponds to the DPh-DNTT film. Similar to the HRTEM analyses, although with a reduced contrast, horizontal lines can be distinguished within the DPh-DNTT film. The periodicity of 2.4 nm again corresponds well to the length of the molecule (c = 2.43 nm), confirming the edge-on orientation of the molecules. The lines with a brighter contrast correspond to the conjugated core of the molecules (DNTT section), which contains S and exhibits a larger mass density compared to the two terminal phenyl substituents, as seen from the HRTEM analyses shown above and the calculation of the projected potential (Figure S3, Supporting Information). Below the DPh-DNTT layer, the AlO_x/SAM gate dielectric, Al gate electrode, and Si substrate layers are seen.

Figure 3b−d shows EDX results obtained from the specimen. Figure 3c shows a HAADF-STEM image, where a blue arrow indicates the position and direction of the elemental intensity line profile shown in Figure 3d. The three rectangles in Figure 3c mark the regions from which the three EDX spectra shown in Figure 3b have been obtained. The spectrum shown in blue, corresponding to the Au layer, shows a strong Au−M peak and some intensity for other elements (C, O, Si), which can be mostly attributed to fluorescence in nearby specimen regions. The EDX spectrum of the DPh-DNTT layer (black line in Figure 3b) shows a strong C−K peak, and also an S−K peak is clearly seen, as expected from the chemical composition of the molecule. The O signal can be attributed to both surface oxidation and a fluorescence signal from the nearby AlO_x gate dielectric. The EDX spectrum taken from the interface between DPh-DNTT and the gate dielectric (red line in Figure 3b) shows strong Al and O peaks, as expected from the AlO_x composition of the gate dielectric, together with C and S peaks with reduced intensity. Again, a Si peak is identified, whose intensity is similar to the Au region when considering that the data for DPh-DNTT and the interface region has been multiplied by a factor of 4, indicating that the signal is not originating from the specimen itself. A minor peak is also found at the position of the P K_α line at an energy of 2 keV, which is attributed to the P atom in the anchor group of the phosphonic acid molecules in the SAM.

In addition to the plot of the three spectra in Figure 3b, the spatial distribution of the elements across the layer system can be seen in Figure 3d. For this, the intensity in the respective peaks was determined and is plotted as a function of the position along the line profile. The Al gate electrode and AlO_x dielectric can be identified from the high Al (light blue line) and O (red) intensities, respectively. The DPh-DNTT film exhibits a constant intensity of C (black line) and S (yellow line). Right at the interface between the gate dielectric and DPh-DNTT, a small intensity is found for P (green line). The Au intensity is found to increase strongly in the vicinity of the

https://doi.org/10.1021/acsami.6c01886
ACS Appl. Mater. Interfaces 2026, 18, 18073−18081

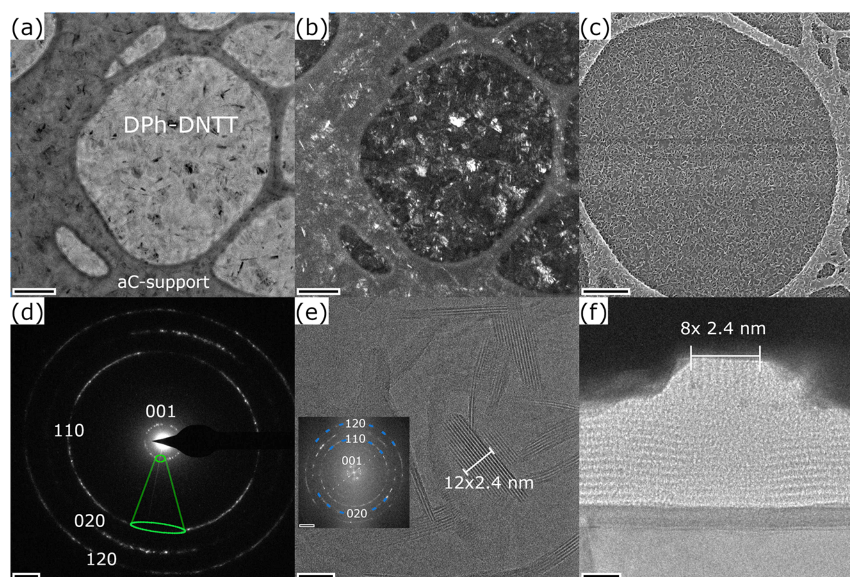

Figure 4. Microstructure analysis using DPh-DNTT plan-view specimens. (a) Bright-field and (b) dark-field TEM images of a DPh-DNTT plan-view specimen. (c) SEM image of the DPh-DNTT layer grown on the TEM grid revealing the typical morphology with numerous protrusions. (d) SAED pattern of the DPh-DNTT thin film showing both [001] and [*hk*0] reflections. (e) HRTEM image revealing both face-on and edge-on configurations of the DPh-DNTT molecules, as seen from the inset FFT. A set of 12 unit cells in the face-on configuration was indicated. (f) HRTEM image of a cross-sectional lamella including a protrusion area. The periodicity of the vertical lines indicates the face-on configuration of the DPh-DNTT molecule, which is limited to the protrusion, as horizontal fringes indicate the edge-on configuration in the underlying layer. Scale bars are (a,b) 300 nm, (c) 1 μm, (d) 1 nm^{-1}, (e) 30 nm, inset FFT 0.8 nm^{-1}, and (f) 10 nm.

Au layer. In addition, P and S intensities are measured, which, however, can be attributed to the peak overlap between the strong Au−M line and the P−K and S−K lines. This overlap is seen in the comparison of EDX spectra in Figure 3b.

Microstructure Analysis

The results shown in the previous section reveal the edge-on orientation of the DPh-DNTT molecules in the first molecular layer located on the surface of the gate dielectric of the TFTs. In addition to these cross-sectional specimens, DPh-DNTT thin films were deposited directly onto TEM grids, which allowed a further analysis of their microstructure. Figure 4 shows the experimental results obtained from TEM analyses of these specimens. The bright-field (BF) TEM image (Figure 4a) reveals several small dark areas, which correspond to grains in which the electron beam undergoes stronger diffraction. The size of these grains is small, in the range 10−100 nm, indicating a nanocrystalline structure of the DPh-DNTT thin film. This agrees with the size of the grains found in the cross-sectional analysis. A similar grain size is seen from the dark-field (DF) TEM image shown in Figure 4b obtained from the identical sample region. The amorphous carbon (aC) support film is visible as a dark (bright) region in the BF (DF) TEM images. Figure 4c shows an SEM image acquired from the DPh-DNTT thin film grown on the TEM grid and reveals the typical morphology of this organic semiconductor,[4] indicating that the growth of the molecule on the aC support of the TEM grid is similar to the growth on the gate dielectric of the organic TFTs discussed in the previous section. Figure S6 (SI) shows an SEM image of the functional DPh-DNTT TFT prior to TEM lamella preparation, revealing a similar morphology.

Figure 4d shows a selected-area electron diffraction (SAED) pattern acquired from a DPh-DNTT plan-view specimen using an SA aperture corresponding to a size of 0.6 μm^2. The presence of multiple spots again confirms the small grain size of the individual grains. The three outer rings seen in the SAED pattern can be linked to [*hk*0] reflections as indicated and correspond to DPh-DNTT grains grown in an edge-on configuration (DPh-DNTT molecules standing upright) on the substrate as expected from the cross-sectional analysis. However, additional reflections show up at lower spatial frequencies, and these reflections can be attributed to the [001] lattice interplanar spacing (c = 2.43 nm). These reflections thus indicate that in the DPh-DNTT film, molecules are found in both face-on and edge-on orientations.

The different reflections are located on rings; however, their distribution on these rings is not homogeneous, and no reflections are found for specific angular ranges (indicated by green elipses). Interestingly, it seems that the angular ranges with missing reflections agree between the [001] and [110] reflections, which suggests that both directions are related to each other. Additional SAED analyses indeed indicate that in many cases, a [001] reflection and a [110] reflection are found under a similar angle (see Figure S7, Supporting Information). A comparison of the [110] and [001] lattice parameters shows that the [001] interplanar spacing c corresponds rather well to five times the [110] lattice distance d_{110}, with a mismatch of 1.5%:

$$c = 2.43 \text{ nm} = 1.015 \cdot 5 \cdot d_{110} = 1.015 \cdot 5 \cdot 0.479 \text{ nm} \quad (1)$$

These observations suggest that the DPh-DNTT molecules with face-on orientation grow in an oriented fashion on top of the [110] direction of an underlying DPh-DNTT thin film with edge-on orientation due to the fact that the lattice mismatch between these two directions is relatively small (1.5%). Such a templated growth has already been observed for large single crystals (MMCs) by X-ray diffraction techniques and is exploited to epitaxially grow organic semiconductor molecules.[26] Here, our results suggest that such templated growth can occur similarly for nanocrystalline vacuum-deposited films.

https://doi.org/10.1021/acsami.6c01886
ACS Appl. Mater. Interfaces 2026, 18, 18073−18081

A HRTEM image of the DPh-DNTT thin film grown on a TEM grid is shown in Figure 4e. The image reveals well-defined areas with a strong fringe contrast, whose periodicity is 2.4 nm. These areas thus correspond to DPh-DNTT molecules in face-on orientation, confirming again that this configuration is present in the DPh-DNTT thin film. The width of 20−30 nm and the elongated shape of these areas with a periodicity of 2.4 nm correspond well to the shape of the protrusions found in the thin-film morphology, suggesting that these protrusions correspond to molecules in the face-on configuration. This is in agreement with recent findings from AFM analyses.[25] The FFT shown as the inset in Figure 4e reveals that in addition to the [00*l*] spots, numerous [*hk*0] spots are present, which are linked to molecules in the edge-on configuration. The HRTEM images were used to obtain a rough estimate of the proportion of molecules in edge-on with respect to face-on configurations. Therefore, the area with face-on molecules was determined by manual selection in a few HRTEM images. Assuming an average thickness of 15 and 30 nm of the face-on and edge-on configurations estimated from cross-sectional analysis, the volume fraction of face-on molecules is estimated to be on the order of 5 vol %.

Figure S8, Supporting Information, shows a TEM analysis of a plan-view specimen of a DPh-DNTT thin film with a reduced layer thickness of nominally 8 nm. For this reduced thickness, the presence of molecules in a face-on configuration is strongly reduced, as indicated by the absence of [001] reflections. Only strongly defocused TEM imaging reveals the presence of a small number of face-on molecules. These results indicate that for this small DPh-DNTT film thickness, the growth of the face-on configuration is still incipient, which strengthens the idea of a templated growth on top of a (continuous) thin film with molecules in an edge-on orientation.

From the TEM analyses of the plan-view specimens, we cannot conclude whether the molecules with a face-on configuration in the thick DPh-DNTT thin film are located within the first molecular layer (i.e., directly on the substrate surface) or on top of edge-on DPh-DNTT molecules. To obtain this information, additional cross-sectional analyses were conducted, specifically focusing on imaging the DPh-DNTT molecules in the protrusion areas. Figure 4f shows an HRTEM image of such a cross-sectional specimen including a protrusion. The image first again confirms the layer structure of the organic TFT (Al, AlO_x/SAM, DPh-DNTT, Au). Second, the edge-on configuration of the DPh-DNTT molecules on top of the AlO_x/SAM gate dielectric is seen from the horizontal fringe contrast, similar to the previous analyses. In addition, vertical fringes with a periodicity of 2.4 nm can be distinguished in the protrusion, confirming the face-on orientation in this area. These vertical fringes are limited to the protrusion, which therefore suggests that the face-on DPh-DNTT molecules indeed grow on top of an underlying film with edge-on molecules. The additional HRTEM images shown in Figure S9 (SI) acquired at different defocus values and from a second protrusion region confirm this specific combination of a face-on configuration located on top of an underlying edge-on configuration of the DPh-DNTT thin film. However, these HRTEM images only allow us to determine the [001] direction of the molecules and therefore cannot be used to gain further information about a possible templated growth suggested by plan-view HRTEM and SAED analyses (Figure 4d,e), requiring further experiments to fully confirm the growth mechanism of the DPh-DNTT films.

CONCLUSIONS

The detailed transmission electron microscopy (TEM) investigations on vacuum-deposited 2,9-diphenyl-dinaphtho-[2,3-b:2′,3′-f]thieno[3,2-*b*]thiophene (DPh-DNTT) organic semiconductor thin films give important insights into their microstructure. Cross-sectional analyses confirm that the first few layers of the organic semiconductor on top of the gate dielectric in organic thin-film transistors (TFTs) exhibit an edge-on configuration of the molecules. Furthermore, a face-on configuration of the molecules is found in the protrusion areas, which grow on top of the underlying thin film with an edge-on configuration. High-resolution imaging and spectroscopy analyses also allow the identification of the *n*-tetradecylphosphonic acid self-assembled monolayer (SAM) that is part of the gate dielectric of the transistors.

Microstructure analyses of the DPh-DNTT thin film reveal a small grain size of less than 100 nm. This small grain size results in the presence of multiple grain boundaries in the thin films. Thereby, adjacent grains show a rotation of the molecular crystal around the [001] axis, implying that molecules are in an edge-on configuration for all grains grown on the gate dielectric. As the DPh-DNTT organic semiconductor exhibits excellent charge-carrier mobilities, these grain boundaries can be expected to have only a small impact on the mobility, which is in contrast to studies of pentacene thin films. SAED patterns obtained on DPh-DNTT thin films suggest that the [001] reflections are linked to the [110] reflections. As there is only a relatively small lattice mismatch between the c and $5d_{110}$ interplanar distances, the DPh-DNTT molecules grown edge-on are assumed to represent a template for the growth of the molecules in the face-on configuration, similar as has been observed for large single-crystalline monolayer molecular crystals (MMCs).[26]

METHODS

Specimen Preparation

Two types of specimen were fabricated: functional DPh-DNTT TFTs on silicon substrates for cross-sectional TEM analysis and DPh-DNTT thin films deposited onto commercial TEM grids (holey carbon + continuous ultrathin carbon film) for plan-view TEM analysis. The TFTs were fabricated on heavily doped silicon substrates in the inverted staggered (bottom-gate, top-contact) device architecture. In the first step, a 30 nm thick layer of aluminum was deposited by thermal evaporation in vacuum at a base pressure of 10^{-7} mbar with a deposition rate of 2.5 nm/s.[34] This unpatterned aluminum layer serves as the gate electrode of the TFTs for current−voltage measurements. The aluminum surface was exposed to an oxygen plasma (oxygen flow rate: 30 sccm; oxygen partial pressure: 10 mTorr; RF power: 200 W; duration: 30 s) to increase the thickness of the native aluminum oxide on the surface of the aluminum gate electrode to about 6 nm. The substrate was then immersed into a 1 mM solution of *n*-tetradecylphosphonic acid in 2-propanol for a duration of 1 h to allow the formation of a self-assembled monolayer (SAM) on the aluminum oxide surface. To stabilize the SAM, the substrate was heated to a temperature of 80 °C for 5 min, resulting in a hybrid AlO_x/SAM gate dielectric with a thickness of about 8 nm and a unit-area capacitance of 700 nF/cm^2.[35] A layer of DPh-DNTT with a nominal thickness of 40 nm was then deposited by thermal sublimation in vacuum with a deposition rate of 0.04 nm/s. During the DPh-DNTT deposition, the substrate was held at a temperature of 90 °C. In the final process step, gold source and drain contacts with a thickness of 30 nm were deposited by thermal evaporation in vacuum with a deposition rate of 0.03 nm/s through a silicon stencil mask.[24] Deposition rates and nominal layer thicknesses were measured by using a quartz-crystal microbalance. The current−voltage character-

https://doi.org/10.1021/acsami.6c01886
ACS Appl. Mater. Interfaces 2026, 18, 18073−18081

istics of the DPh-DNTT TFTs were recorded using an Agilent 4156C Semiconductor Parameter Analyzer in ambient air at room temperature. An additional specimen following the same recipe was prepared but with a nominal thickness of the DPh-DNTT film of 8 nm. For plan-view TEM analysis, a layer of DPh-DNTT with a nominal thickness of 50 nm (8 nm for a second specimen) was deposited by thermal sublimation in vacuum with a deposition rate of 0.04 nm/s, and the substrate was held at a temperature of 90 °C.

A schematic cross-section of the TFT and measured current−voltage characteristics of the studied functional DPh-DNTT TFT are shown in Figure S1 (SI).

Electron Microscopy

A Titan[3] (Thermo Fisher Scientific) transmission electron microscope was used for conducting high-resolution (HR)TEM and SAED analyses of the DPh-DNTT specimens. The microscope is equipped with a field-emission gun, operated at 300 keV, a monochromator, and an aberration corrector for the imaging lens system. A XF416(R) CMOS camera (TVIPS GmbH) was used to acquire TEM images and SAED patterns. SAED patterns were acquired under electron doses well below 2 $e^{-}Å^{-2}$, while it was increased to up to approximately 25 $e^{-}Å^{-2}$ for high-resolution (HR)TEM imaging.

Furthermore, a double-corrected Themis Z microscope (Thermo Fisher Scientific) was used for STEM imaging and STEM-EDX. EDX was performed using a Super X 4-quadrant detector. The STEM convergence angle was 30 mrad, and the HAADF collection angle was 62 mrad.

ReciPro software has been used to calculate the projected potentials of the DPh-DNTT crystal.[36]

While the DPh-DNTT thin films directly grown on the TEM grids were investigated as is, a Helios G4 (Thermo Fisher Scientific) dual-beam machine with combined focused ion beam (FIB) and scanning electron microscopy (SEM) was employed to prepare two TEM lamellae from the functional DPh-DNNT organic TFTs following a standard procedure. While this standard procedure typically leads to the amorphization of many molecular crystals (e.g., of pentacene) as seen both in literature[20] and in recent own works, the DPh-DNTT organic semiconductor remained crystalline, which is attributed to its high-temperature stability.[23]

■ ASSOCIATED CONTENT

Data Availability Statement

The data (images, spectroscopy, and graph data) are freely available on Zenodo: 10.5281/zenodo.17344166.

Supporting Information

The Supporting Information is available free of charge at https://pubs.acs.org/doi/10.1021/acsami.6c01886.

Supporting electron microscopy data and an electrical characterization of the studied functional DPh-DNTT TFT (PDF)

■ AUTHOR INFORMATION

Corresponding Author

Simon Hettler − *Laboratory for Electron Microscopy, Karlsruhe Institute of Technology, 76131 Karlsruhe, Germany;* orcid.org/0000-0002-9102-7895; Email: simon.hettler@kit.edu

Authors

Ute Zschieschang − *Max Planck Institute for Solid State Research, 70569 Stuttgart, Germany*

Hagen Klauk − *Max Planck Institute for Solid State Research, 70569 Stuttgart, Germany;* orcid.org/0000-0003-4563-5635

Martin Peterlechner − *Laboratory for Electron Microscopy, Karlsruhe Institute of Technology, 76131 Karlsruhe, Germany*

Yolita M. Eggeler − *Laboratory for Electron Microscopy, Karlsruhe Institute of Technology, 76131 Karlsruhe, Germany*

Complete contact information is available at: https://pubs.acs.org/10.1021/acsami.6c01886

Author Contributions

M.P., Y.M.E., and H.K. designed the study. U.Z. and H.K. fabricated and electrically characterized the TFTs. S.H. performed TEM experiments and related data analysis and wrote the original draft. The manuscript was revised by all authors.

Notes

The authors declare no competing financial interest.

■ ACKNOWLEDGMENTS

Funding by the German Research Foundation (DFG) through the collaborative research center CRC 1249 "N-Heteropolycycles as Functional Materials" (Project Number 281029004-SFB 1249, projects C01 and C12) is gratefully acknowledged. The authors would like to thank Kazuo Takimiya (RIKEN Center for Emergent Matter Science, Wako, Saitama, Japan) as well as Koichi Ikeda, Yuichi Sadamitsu, and Satoru Inoue (Nippon Kayaku, Tokyo, Japan) for providing the organic semiconductor DPh-DNTT. This work was partly carried out with the support of the Karlsruhe Nano Micro Facility (KNMFi, www.knmf.kit.edu), a Helmholtz Research Infrastructure at the Karlsruhe Institute of Technology (KIT, www.kit.edu). Help of Di Wang (KNMFi) with STEM-EDX data acquisition is acknowledged.

■ REFERENCES

(1) Sekitani, T.; Zschieschang, U.; Klauk, H.; Someya, T. Flexible organic transistors and circuits with extreme bending stability. *Nat. Mater.* **2010**, *9*, 1015−1022.

(2) Okamoto, T.; Kumagai, S.; Fukuzaki, E.; Ishii, H.; Watanabe, G.; Niitsu, N.; Annaka, T.; Yamagishi, M.; Tani, Y.; Sugiura, H.; Watanabe, T.; Watanabe, S.; Takeya, J. Robust, high-performance n-type organic semiconductors. *Sci. Adv.* **2020**, *6*, No. eaaz0632.

(3) Mottaghi, M.; Horowitz, G. Field-induced mobility degradation in pentacene thin-film transistors. *Org. Electron.* **2006**, *7*, 528−536.

(4) Hofmockel, R.; Zschieschang, U.; Kraft, U.; Rödel, R.; Hansen, N. H.; Stolte, M.; Würthner, F.; Takimiya, K.; Kern, K.; Pflaum, J.; Klauk, H. High-mobility organic thin-film transistors based on a small-molecule semiconductor deposited in vacuum and by solution shearing. *Org. Electron.* **2013**, *14*, 3213−3221.

(5) Dreher, M.; Bischof, D.; Widdascheck, F.; Huttner, A.; Breuer, T.; Witte, G. Interface Structure and Evolution of Dinaphthothienothiophene (DNTT) Films on Noble Metal Substrates. *Adv. Mater. Interfaces* **2018**, *5*, No. 1800920.

(6) Zhang, J.; Guo, J.; Zhang, H.; Liu, J.; You, S.-Y.; Jiang, L. Solution-Processed Monolayer Molecular Crystals: From Precise Preparation to Advanced Applications. *Precision Chemistry* **2024**, *2*, 380−397.

(7) Martin, D. C.; Chen, J.; Yang, J.; Drummy, L. F.; Kübel, C. High resolution electron microscopy of ordered polymers and organic molecular crystals: Recent developments and future possibilities. *J. Polym. Sci., Part B: Polym. Phys.* **2005**, *43*, 1749−1778.

(8) Minakata, T.; Imai, H.; Ozaki, M.; Saco, K. Structural studies on highly ordered and highly conductive thin films of pentacene. *J. Appl. Phys.* **1992**, *72*, 5220−5225.

(9) Hayashida, M.; Kawasaki, T.; Kimura, Y.; Takai, Y. Estimation of suitable condition for observing copper−phthalocyanine crystalline film by transmission electron microscopy. *Nuclear Instruments and Methods in Physics Research Section B: Beam Interactions with Materials and Atoms* **2006**, *248*, 273−278.
(10) Qian, H.; Malac, M.; Egerton, R. Microscopy of pentacene thin films. *Philos. Mag.* **2007**, *87*, 253−266.
(11) Haas, B.; Beyer, A.; Witte, W.; Breuer, T.; Witte, G.; Volz, K. Application of transmission electron microscopy for microstructural characterization of perfluoropentacene thin films. *J. Appl. Phys.* **2011**, *110*, No. 073514.
(12) Wang, J.; Ren, Z.; Yan, T.; Jia, R.; Cheng, Y.; Zhang, X.; Jie, J. Floating Epitaxy and Stitching Growth of Bilayer Organic Semiconductor Single Crystals on Polymer Dielectric Toward High-Performance and Ultra-Flexible Transistors. *Adv. Mater.* **2026**, *38*, No. e15477.
(13) Dürr, A.; Schreiber, F.; Kelsch, M.; Dosch, H. Optimized preparation of cross-sectional TEM specimens of organic thin films. *Ultramicroscopy* **2003**, *98*, 51−55.
(14) Dürr, A. C.; Schreiber, F.; Kelsch, M.; Carstanjen, H. D.; Dosch, H.; Seeck, O. H. Morphology and interdiffusion behavior of evaporated metal films on crystalline diindenoperylene thin films. *J. Appl. Phys.* **2003**, *93*, 5201−5209.
(15) Kirmse, H.; Oehlschlegel, E.; Polzer, F.; Blumstengel, S.; Sparenberg, M.; Henneberger, F. Cross-sectional TEM preparation of hybrid inorganic/organic materials systems by ultramicrotomy. *Journal of Physics: Conference Series* **2013**, *471*, No. 012034.
(16) Murakami, Y.; Tomiya, S.; Koshitani, N.; Kudo, Y.; Satori, K.; Itabashi, M.; Kobayashi, N.; Nomoto, K. Microstructural Study of the Polymorphic Transformation in Pentacene Thin Films. *Phys. Rev. Lett.* **2009**, *103*, No. 146102.
(17) Gilchrist, J. B.; Basey-Fisher, T. H.; Chang, S. C.; Scheltens, F.; McComb, D. W.; Heutz, S. Uncovering Buried Structure and Interfaces in Molecular Photovoltaics. *Adv. Funct. Mater.* **2014**, *24*, 6473−6483.
(18) Gilchrist, J. B.; Heutz, S.; McComb, D. W. Revealing structure and electronic properties at organic interfaces using TEM. *Curr. Opin. Solid State Mater. Sci.* **2017**, *21*, 68−76.
(19) Bassim, N.; De Gregorio, B.; Kilcoyne, A.; Scott, K.; Chou, T.; Wirick, S.; Cody, G.; Stroud, R. Minimizing damage during FIB sample preparation of soft materials. *J. Microsc.* **2012**, *245*, 288−301.
(20) Sekitani, T.; Yokota, T.; Zschieschang, U.; Klauk, H.; Bauer, S.; Takeuchi, K.; Takamiya, M.; Sakurai, T.; Someya, T. Organic Nonvolatile Memory Transistors for Flexible Sensor Arrays. *Science* **2009**, *326*, 1516−1519.
(21) Kang, M. J.; Miyazaki, E.; Osaka, I.; Takimiya, K.; Nakao, A. Diphenyl Derivatives of Dinaphtho[2,3-b:2,3-f]thieno[3,2-b]-thiophene: Organic Semiconductors for Thermally Stable Thin-Film Transistors. *ACS Appl. Mater. Interfaces* **2013**, *5*, 2331−2336.
(22) Niimi, K.; Kang, M. J.; Miyazaki, E.; Osaka, I.; Takimiya, K. General Synthesis of Dinaphtho[2,3-b:2,3-f]thieno[3,2-b]thiophene (DNTT) Derivatives. *Org. Lett.* **2011**, *13*, 3430−3433.
(23) Yokota, T.; Kuribara, K.; Tokuhara, T.; Zschieschang, U.; Klauk, H.; Takimiya, K.; Sadamitsu, Y.; Hamada, M.; Sekitani, T.; Someya, T. Flexible Low-Voltage Organic Transistors with High Thermal Stability at 250°C. *Adv. Mater.* **2013**, *25*, 3639−3644.
(24) Wollandt, T.; Steffens, S.; Radiev, Y.; Letzkus, F.; Burghartz, J. N.; Witte, G.; Klauk, H. Reliability of the Transmission Line Method and Reproducibility of the Measured Contact Resistance of Organic Thin-Film Transistors. *ACS Nano* **2025**, *19*, 9915−9924.
(25) Yan, L.; Zou, D.; Yin, Y.; Guo, Y.; Chen, M.; Cheng, X.; Chan, P. K. L. The Nanosprouts Structural Inhomogeneity of Organic Semiconductors and the Optical Memory Properties. *Adv. Mater. Technol.* **2025**, *10*, No. e00197.
(26) Peng, B.; Jiao, X.; Ren, X.; Chan, P. K. L. Epitaxy of an Organic Semiconductor Templated by Molecular Monolayer Crystals. *ACS Applied Electronic Materials* **2021**, *3*, 752−760.
(27) Kraft, U.; Takimiya, K.; Kang, M. J.; Rödel, R.; Letzkus, F.; Burghartz, J. N.; Weber, E.; Klauk, H. Detailed analysis and contact properties of low-voltage organic thin-film transistors based on dinaphtho[2,3-b:2,3-f]thieno[3,2-b]thiophene (DNTT) and its didecyl and diphenyl derivatives. *Org. Electron.* **2016**, *35*, 33−40.
(28) Malac, M.; Hettler, S.; Hayashida, M.; Kawasaki, M.; Konyuba, Y.; Okura, Y.; Iijima, H.; Ishikawa, I.; Beleggia, M. Computer simulations analysis for determining the polarity of charge generated by high energy electron irradiation of a thin film. *Micron* **2017**, *100*, 10−22.
(29) Jedaa, A.; Burkhardt, M.; Zschieschang, U.; Klauk, H.; Habich, D.; Schmid, G.; Halik, M. The impact of self-assembled monolayer thickness in hybrid gate dielectrics for organic thin-film transistors. *Org. Electron.* **2009**, *10*, 1442−1447.
(30) Fukuda, K.; Hamamoto, T.; Yokota, T.; Sekitani, T.; Zschieschang, U.; Klauk, H.; Someya, T. Effects of the alkyl chain length in phosphonic acid self-assembled monolayer gate dielectrics on the performance and stability of low-voltage organic thin-film transistors. *Appl. Phys. Lett.* **2009**, *95*, 203301.
(31) Horowitz, G. Organic Field-Effect Transistors. *Adv. Mater.* **1998**, *10*, 365−377.
(32) Sun, Y.; Liu, Y.; Zhu, D. Advances in organic field-effect transistors. *J. Mater. Chem.* **2005**, *15*, 53.
(33) Deepak, F. L.; Mayoral, A.; Arenal, R., Eds. *Advanced Transmission Electron Microscopy*; Springer eBook Collection; Springer: Cham, 2015. 27217793 pp.
(34) Geiger, M.; Acharya, R.; Reutter, E.; Ferschke, T.; Zschieschang, U.; Weis, J.; Pflaum, J.; Klauk, H.; Weitz, R. T. Effect of the Degree of the Gate-Dielectric Surface Roughness on the Performance of Bottom-Gate Organic Thin-Film Transistors. *Adv. Mater. Interfaces* **2020**, *7*, No. 1902145.
(35) Geiger, M.; Hagel, M.; Reindl, T.; Weis, J.; Weitz, R. T.; Solodenko, H.; Schmitz, G.; Zschieschang, U.; Klauk, H.; Acharya, R. Optimizing the plasma oxidation of aluminum gate electrodes for ultrathin gate oxides in organic transistors. *Sci. Rep.* **2021**, *11*, 6382.
(36) Seto, Y.; Ohtsuka, M. ReciPro: free and open-source multipurpose crystallographic software integrating a crystal model database and viewer, diffraction and microscopy simulators, and diffraction data analysis tools. *J. Appl. Crystallogr.* **2022**, *55*, 397−410.

CAS BIOFINDER DISCOVERY PLATFORM™
CAS BIOFINDER HELPS YOU FIND YOUR NEXT BREAKTHROUGH FASTER
Navigate pathways, targets, and diseases with precision
Explore CAS BioFinder

https://doi.org/10.1021/acsami.6c01886
ACS Appl. Mater. Interfaces 2026, 18, 18073−18081